Environ. Sci. Technol. **2006**, *40,* 3336−3341

Quantifying Stream−Aquifer Interactions through the Analysis of Remotely Sensed Thermographic Profiles and In Situ Temperature Histories

STEVEN P. LOHEIDE II* AND
STEVEN M. GORELICK

Department of Geological and Environmental Sciences, Stanford University, Stanford, CA 94305-2115

The interaction between surface and subsurface waters through hyporheic exchange and baseflow is critical to maintaining ecological health in streams. During warm periods, groundwater−surface water interactions have two primary effects on stream temperature: (1) cool groundwater discharging as baseflow lowers stream temperature and (2) hyporheic exchange buffers diurnal stream temperature variations. We demonstrate, for the first time, how high-resolution, remotely sensed forward-looking infrared (FLIR) images and instream temperature data can be used to quantify detailed spatial patterns of groundwater discharge to a 1.7 km reach of Cottonwood Creek in Plumas National Forest, CA. We quantify the individual effects of baseflow and hyporheic exchange on stream temperatures by simulating the stream energy budget under different conceptual models of the stream−aquifer interaction. Observed spatial and temporal patterns of stream temperature are consistent with an increase in baseflow and hyporheic exchange within the middle, restored stream reach when compared to groundwater fluxes in the surrounding, unrestored reaches. One implication is that pond and plug stream restoration may improve the aquatic habitat by depressing maximum stream temperatures by >3 °C (K).

Introduction

Hydrologists, stream ecologists, aquatic chemists, and water resource managers are often unable to quantify water and thermal fluxes across the streambed interface, even though these exchanges administer significant control on relevant physical and chemical processes (*1*, *2*, *3*). For instance, groundwater discharge to streams accumulates throughout a watershed's drainage network as baseflow, which supports river flow during dry periods, maintains aquatic ecosystems, and is critical to humans for water supply and agriculture. Hyporheic water flow from the stream into the subsurface and back to the stream plays important roles in thermal buffering, nutrient cycling, and stream ecology (*1*, *4*, *5*). Direct measurement of groundwater discharge to a stream at a point is challenging, and obtaining representative point measurements throughout a watershed is a practical impossibility. Understanding, protecting, and restoring the hydrologic function and ecosystem services provided by baseflow and hyporheic exchanges requires better methods for quantifying these spatially distributed fluxes.

* Corresponding author phone: (650)725-8070; fax: (650) 724-0979; e-mail: sloheide@stanford.edu.

Commercial availability of forward-looking infrared (FLIR) cameras has made it feasible to monitor stream temperature (T_s) from helicopter-based platforms (*6*). High-resolution thermal data can be used for the identification and protection of thermal refugia for fisheries (*7*) and may provide clues about surface water−groundwater interactions (*8*, *9*). For example, stream reaches with high groundwater contributions have lower daily maximum temperatures during the summer months because groundwater remains cool relative to the stream. We present a new method to quantify both groundwater discharge (baseflow) and hyporheic exchange that relies on the detailed thermal signature in the stream over space and time.

The method involves collecting airborne thermographic imagery to obtain longitudinal profiles of T_s at various times during the day and recording instream temperature at selected locations. These thermal profiles and histories are then simulated with a modified version of an existing, one-dimensional (1-D) energy budget/transport model (*10*). Input parameters such as meteorological conditions, vegetative shading characteristics, and stream characteristics were measured on-site, estimated from aerial photographs, and extracted from existing databases. The rates of groundwater inflow and hyporheic exchange were systematically varied until the modeled T_s matched both the in situ and the remotely sensed observations.

The methodology developed here was applied to a 1.67 km reach of Cottonwood Creek in Plumas National Forest, CA (Figure 1). This reach runs through Big Flat, a meadow that was restored in 1995 to reestablish the hydrologic regime and natural vegetation. The meadow had been adversely affected by stream incision, which had caused subsequent meadow dewatering, a change in the hydrologic regime, and a succession from native wet meadow vegetation to sagebrush and dryland grasses (*11*, *12*). This is likely a result of increased erosion caused by land-use practices such as grazing and logging. The pond-and-plug restoration technique involved excavating ponds along the incised channel and filling in the old channel neighboring these ponds (*11*, *12*). The stream was rerouted from the old, deeply incised channel into a newly constructed, unincised, Rosgen type "E" (*13*) channel, to which pool and riffle treatment was performed in 2004. The restoration objective of raising the water table (1) promoted a reestablishment of wet meadow vegetation and (2) increased groundwater flow to the stream through baseflow augmentation (*14*). Groundwater flow into the stream is from regional aquifers and the seasonal drainage of meadow sediments. Hyporheic flow is the local scale exchange of water between the stream and the hyporheic zone on short time scales. The work presented is being used to evaluate the effectiveness of baseflow augmentation.

Methodology

On June 3, 2005, thermal imagery was collected over Cottonwood Creek in Big Flat using methods similar to those used by Torgersen et al. (*15*). A S65 FLIR camera was held in a near vertical position with a manually steered mount beneath a helicopter that flew over the reach, in a downstream direction, four times throughout the day. The camera has a spectral range of 7.5−13 μm and a 24 × 18° field of view. The flight times were 7:43 am, 11:53 am, 4:08 pm, and 7:38 pm. The helicopter altitude was ∼120−160 m, resulting in image resolution of 0.16−0.21 m. Longitudinal profiles of T_s for each flight were created by sampling an approximately circular footprint of 0.3−1.2 m^2 consisting of an average of 9−30 neighboring pixels from the thermal images at intervals

10.1021/es0522074 CCC: $33.50
Published on Web 04/13/2006

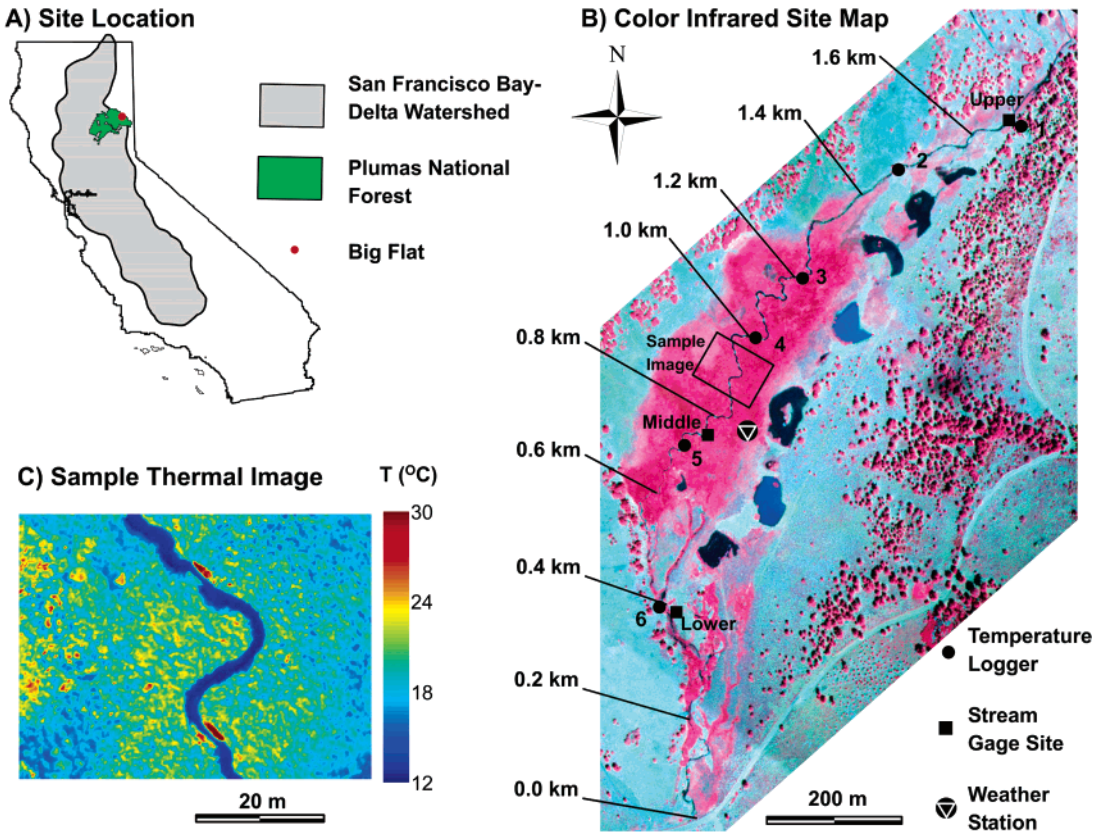

FIGURE 1. (A) Location of Big Flat in the Plumas National Forest, CA. (B) Color infrared base map of Big Flat shows healthy vegetation in pink/red and locations of stream temperature loggers, stream discharge measurements, and the weather station. Stream kilometer is measured upstream from the road crossing. The ponds on the eastern flank of the meadow were created during the restoration and mark the position of the former stream channel. (C) FLIR image showing temperature with a spatial resolution of ~18 cm. Other thermal images in the literature show springs that discharge cool water as a point source (i.e., Figure 1.7 in ref 10); however, in this study, we are interested in diffuse groundwater inflow, which is not visible in a single image but affects T_s at the reach scale.

of ~25 m. Since each flight lasted ~56 s through this reach, the resulting longitudinal profiles of T_s represent a nearly instantaneous snapshot.

Ground-based data served to crosscheck the thermography data, support the stream temperature model, and validate results. Stream bankfull width was measured at ~18 m intervals from stream kilometer 0.39 to 1.33 and was estimated elsewhere from aerial photographs. Streamflow measurements were taken at three locations using an acoustic Doppler velocimeter (SonTec). Instream temperature loggers (HOBO Water Temp Pro v1) recorded T_s at 15−30 min intervals at six locations (Figure 1).

Stream temperature was modeled using HeatSource V7.0, which is distributed at www.deq.state.or.us/wq/TMDLs/WQAnalTools.htm. Except where noted, the procedures outlined by Boyd and Casper (*10*) were used. This finite-difference model solves the 1-D, transient advection−dispersion equation. The model was modified to solve a more general, nonuniform form of this equation:

$$A\frac{\partial T_s}{\partial t} = -\frac{\partial (QT_s)}{\partial x} + \frac{\partial}{\partial x}\left(AD\frac{\partial T_s}{\partial x}\right) + \frac{W\Phi_{net}}{\rho C_p} \qquad (1)$$

In eq 1, T_s is the stream temperature [K]; t is time [s]; x is the distance downstream [m]; $A = A(x)$ is the cross sectional stream area [m^2]; Q is the streamflow [m^3/s]; D is the dispersion coefficient [m^2/s]; ρ is the density of water [kg/m^3]; C_p is the specific heat of water [J/K/kg]; $W = W(x)$ is the stream width [m]; and $\Phi_{net} = \Phi_{net}(x)$ is the net heat flux [J/s/m^2]. The Φ_{net} term accounts for the heat fluxes illustrated in Figure 2. The incoming shortwave solar loading (Φ_{solar})

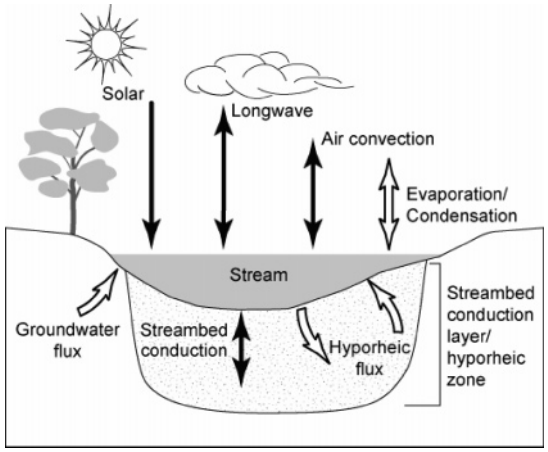

FIGURE 2. Heat exchange mechanisms affecting stream temperature.

reaching the stream surface is calculated based on geographic location, time of year, time of day, cloudiness, and topographic/vegetative shade. Cloudiness is calculated using the maximum predicted solar radiation and the actual solar radiation measured at the weather station (*16*); because we back-calculated cloudiness in this manner, the modeled shortwave radiation is, by definition, equivalent to the measured values. The longwave radiation ($\Phi_{longwave}$) is based on the difference between incoming longwave radiation from the atmosphere and back radiation emitted from the stream. Streambed conduction ($\Phi_{streambed}$) is driven by the temperature gradient between the stream and the streambed conduction layer (Figure 2). Similarly, the sensible heat flux

TABLE 1. Source of Data Required for Stream Temperature Modeling

data type	data source
vegetation shading	vegetation mapped from USGS digital ortho quads
topographic shading	10m USGS digital elevation models
stream slope	10m USGS digital elevation models[a]
bankfull width	measured on the ground and estimated from aerial photographs
stream velocity, width, and depth	modeled using Muskingum–Cunge flow routing in HeatSource
dispersion coefficient	estimated from streamflow, dimensions, and roughness (*10*)
sediment thermal properties	estimated based on porosity
groundwater temperature	measured at various locations within the meadow
cloudiness	recorded at weather station
air temperature	recorded at weather station
humidity	recorded at weather station
wind speed	recorded at weather station
discharge bound. condition	measured (acoustic Doppler velocimeter)
temperature bound. condition	measured (HOBO instream temperature logger)
groundwater inflow	estimated through calibration
hyporheic exchange	estimated through calibration

[a] In heavily vegetated areas, along streams in steep canyons, or when very fine scale variations in slope are required, digital elevation model (DEM) data may not provide a sufficiently accurate estimation of slope. Methods used here to determine slope can be found on pages 140 and 149 of ref 10.

($\Phi_{convection}$) is driven by air convection above the stream and is directly related to the stream–air temperature gradient. The latent heat flux (Φ_{evap}) is a result of evaporation from the stream surface and is calculated with the mass transfer approach based on the water vapor pressure gradient and a wind function. To solve eq 1, input data were specified at 2 m intervals, and computations were performed with a 5 m discretization and a 1 min time step.

We modified the model components that calculate heat fluxes due to groundwater flow (Φ_{gw}) and hyporheic exchanges (Φ_{hyp}). We specified the hyporheic flux rate (q_{hyp}) as a volumetric flux per unit length of stream, [m^2/s]. The heat flux to/from the stream was then calculated as

$$\Phi_{hyp} = \frac{(T_{hyp} - T_s)q_{hyp}\rho C_p}{W} \quad (2)$$

where T_{hyp} is the hyporheic zone temperature. The hyporheic zone is assumed to have the same dimensions and temperature as the conductive layer. The hyporheic zone/conductive layer temperature is modeled by summing the streambed conduction and hyporheic heat fluxes to this zone and calculating the temperature change based on this zone's volume and heat capacity. This modification overcame the inherent difficulty in estimating mass exchange from hydraulic conductivity and hydraulic head gradient estimates. In addition, we better accounted for the heat flux of groundwater inflow (Φ_{gw}) as

$$\Phi_{gw} = \frac{(T_{gw})q_{gw}\rho C_p}{W} \quad (3)$$

where the groundwater inflow (q_{gw}) is the volumetric flux per unit length of the stream, and T_{gw} is the groundwater temperature. This was necessary because the effect of groundwater inflow on stream temperature was previously calculated using a simple, flow-weighted mixing model, which failed to represent the effect of groundwater inflow when small time steps were used.

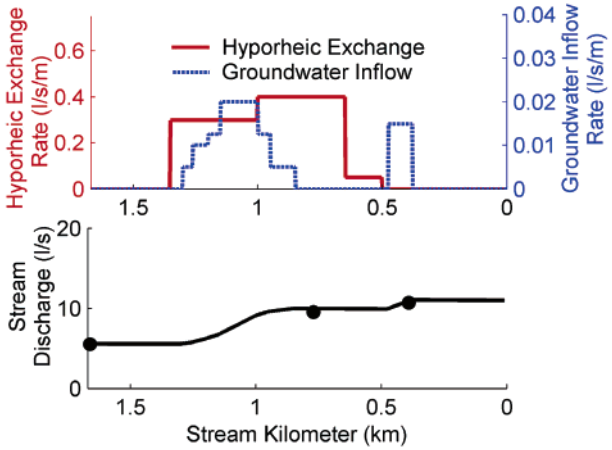

FIGURE 3. Distribution of groundwater inflow and hyporheic exchange, which resulted in the best-fit between the observed and simulated stream temperatures. Where the hyporheic exchange rates are 0.05, 0.3, and 0.4 L/s/m, the depths of the hyporheic zone are 0.25, 0.30, and 0.45 m, respectively. The lower graph shows measured and modeled stream discharge for the cases that include groundwater inflow.

The data requirements and sources are summarized in Table 1. The rates of groundwater inflow and hyporheic exchange and the spatial distribution of these fluxes were varied manually until the best-fit between the modeled and observed T_s was obtained. To evaluate the goodness of fit, we simultaneously compared the diurnal temperature patterns (instream HOBO) and the longitudinal temperature profiles (FLIR) to the model results using both visual inspection and root-mean-square residuals (RMSRs). Three additional cases are considered to demonstrate the effect that groundwater inflow and hyporheic exchanges have on T_s. The best-fit model will be called the "base case" (Figure 3). The second case (No Hyp) is the base case but with no hyporheic exchanges. The third case (No GW) is the base case but neglects all groundwater inflow. The last case (No GW and No Hyp) assumes that there is neither groundwater inflow nor hyporheic exchange anywhere within the reach.

Results and Discussion

Data collected from thermal imagery and instream data loggers are shown in Figures 4 and 5. FLIR-based T_s estimates correlate well with values recorded instream ($R^2 = 0.96$). The mean absolute difference between the two types of data was 0.55 °C (K). The longitudinal profiles demonstrate that heat exchange processes throughout the reach change quite rapidly over space.

The average width and depth of this stream reach are 1.6 ± 0.7 and 0.23 ± 0.18 m, respectively. For discussion purposes, the meadow will be separated into three subreaches: the upper (km 1.67–1.35), middle (km 1.35–0.65), and lower (km 0.65–0). The middle subreach is the zone most directly affected by restoration efforts. In the color infrared image that serves as a base map for Figure 1, riparian vegetation in the middle subreach appears red because the region is dominated by lush mesic vegetation such as sedges and rushes, which indicate a shallow water table. The upper and lower reaches are outside the direct zone of influence of restoration and contain a mix of dryland grasses and sagebrush, which appear blue in the color infrared image. The upper-reach streambed is often intact bedrock or bedrock covered with a thin layer of gravel. The lower-reach streambed is composed of either fine-grained silts or bedrock. Through the middle subreach, the channel was constructed by

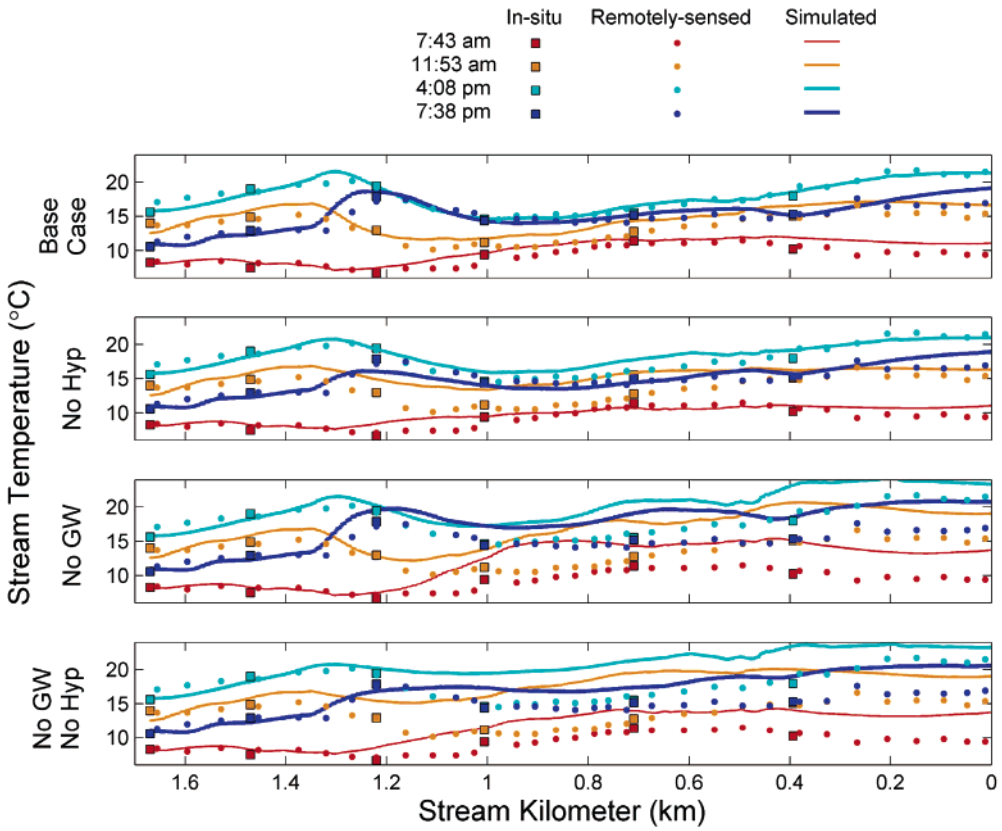

FIGURE 4. Comparison of observed in situ (HOBO) and remotely sensed (FLIR) T_s with simulated longitudinal profiles of T_s. Streamflow is from stream kilometer 1.67 to 0.0 (left to right). The RMSR for the four cases (Base Case, No Hyp, No GW, and No GW−No Hyp) are 1.1, 1.4, 3.3, and 3.5 K, respectively.

excavating the silty meadow soils, which contain zones of sand and gravel. Since channel construction in 1995, sand and gravel have been deposited within the channel both naturally and during restoration. In addition, riprap riffle structures have been added to stabilize the channel and create pools, which raise the elevation of the stream surface. These coarse-grained materials appear to act as important stream−aquifer exchange zones.

Depressed river temperatures indicate streamflow contributions by groundwater (baseflow) and/or hyporheic exchanges. During early June, T_s (∼7−19 °C) is generally greater than the relatively constant groundwater temperature (∼7 ± 0.8 °C). Thus, groundwater inflow within a reach will have a cooling effect on the longitudinal T_s profile either causing T_s to decrease through the reach, or causing T_s to increase to a lesser extent than it would in the absence of baseflow. The effect of groundwater inflow on the longitudinal T_s profile is greater in the afternoon since the temperature difference between the stream and the groundwater is greatest at this time. Hyporheic flows have a buffering effect on T_s in that they tend to cool the stream at times when T_s is rising, but they warm the stream when it is cooling (*17*). Hyporheic buffering causes suppressed T_s maxima, increased minima, and a time lag in the occurrence of stream temperature extrema. The time lag in peak T_s results from the time needed to heat the water and sediments of the hyporheic zone, which are engaged in active heat exchange with the stream.

In both the upper and lower subreaches, T_s increases rapidly in both space (Figure 4) and time (Figure 5) from sunrise until early afternoon as water flows through these reaches. Compared to the upper and lower subreaches, in the middle subreach T_s is buffered and reaches a lower daily maximum, which occurs later in the day. In fact, at sites 1, 2, 3, 4, 5, and 6, the maximum stream temperatures are 16.3, 19.2, 19.9, 14.8, 15.8, and 18.1 °C, occurring at 2:15, 3:30, 5:00, 5:15, 5:45, and 3:30 pm, respectively. The timing and magnitude of these temperature maxima reflect the heat exchange mechanisms occurring at and upstream of these sites; these observations suggest increased baseflow and hyporheic exchange within the middle subreach.

Higher rates of groundwater inflow and hyporheic exchange cause the afternoon dip in the T_s profile (Figure 5) through the middle subreach. Maximum daily T_s in the upper reach (sites 1 and 2) and the lower reach (site 6) are fully 2−3 degrees higher than those in the middle reach (sites 4 and 5), a result primarily of the cooling influence of inflowing groundwater. Yet, hyporheic exchange also contributes to the lower T_s by moderating daily T_s extremes. A more diagnostic effect of increased hyporheic exchange is that the maximum T_s occurs ∼2 h later in the middle subreach versus the other subreaches. This effect is seen in the temporal data (Figure 5) by comparing the observed diurnal temperature records at sites 1, 2, and 6 with the muted and lagged patterns observed at sites 4 and 5. The diurnal temperature record at site 3 (just downstream of the transition into the restored reach) has a high maximum because of the influence of the upper reach, yet also experiences a significant lag caused by a high rate of hyporheic exchange immediately upstream. This hyporheic exchange retards heat advection.

Simulating T_s and heat exchange processes provided quantitative estimates of groundwater contributions to streamflow and hyporheic exchange rates. These fluxes were determined by varying groundwater inflow rates, hyporheic exchange rates, hyporheic zone depth, and the distribution of these fluxes until the simulated temperatures matched the observed spatial and temporal T_s data. The matches were compared using the RMSR (see captions of Figures 4 and 5). The best-fit model was obtained using the groundwater inflow and exchange rates in Figure 3. The RMSR between the

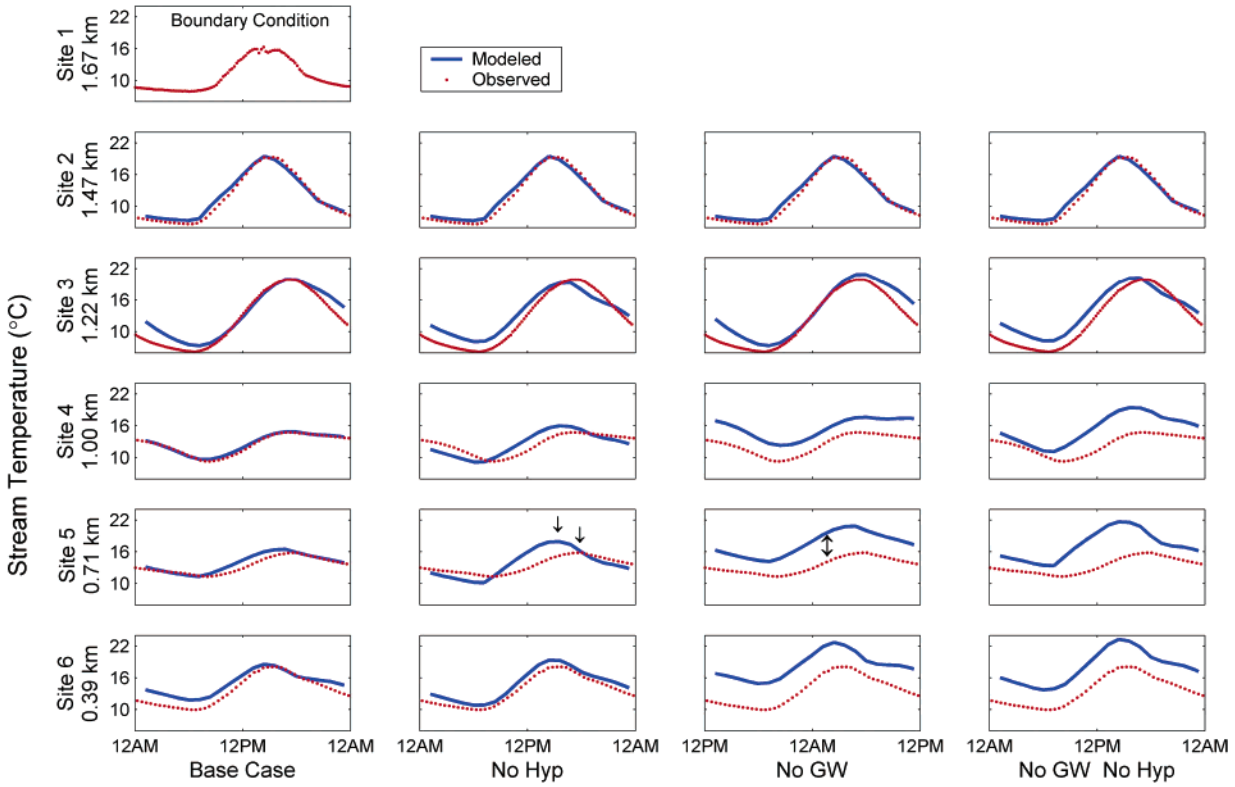

FIGURE 5. Simulated and observed diurnal records of T_s at the locations of the instream temperature loggers for the four cases. Data from Site 1 was used as the upstream boundary condition. The RMSR for the data at the other five sites for the Base, No Hyp, No GW, and No GW—No Hyp cases are 1.1, 1.4, 3.2, and 3.2 K, respectively. The two downward arrows highlight the discrepancy between the modeled and observed times of maximum T_s when hyporheic flow is neglected. The double-ended arrow emphasizes that T_s is overpredicted when groundwater inflow is neglected.

simulated T_s and the FLIR longitudinal profiles is 1.1 K. The RMSR between the simulated T_s and the HOBO-recorded diurnal T_s patterns is also 1.1 K. Checking against the independent measurement of groundwater contributions obtained with synoptic stream gaging (Figure 3), we note that the increase in streamflow attributed to groundwater inflow as determined here agrees with the spatially integrated values provided by gaging. Streamflow measured at the upper, middle, and lower stream gage sites were 0.0055, 0.0095, and 0.0107 m^3/s, respectively; modeled values were 0.0055, 0.0099, and 0.0108 m^3/s, respectively.

When hyporheic exchange is neglected, less buffering of T_s occurs, and the RMSR increases by 0.3 °C (K) for both the longitudinal (Figure 4) and temporal (Figure 5) data sets. A large discrepancy occurs at site 5 in the No Hyp case (Figure 5) because the temperature record at this site is strongly affected by heat exchange processes occurring immediately upstream in the middle subreach, where neglecting hyporheic exchanges has the greatest impact. Neglecting hyporheic exchanges causes the temperature maximum to be overpredicted by 2.0 °C (K) and to occur 2.5 h earlier in the day in the downstream portion of the middle subreach (site 5).

When groundwater inflow is neglected, simulated T_s is too high in the middle and lower subreaches, with the cumulative error becoming more severe downstream. In this case, the RMSR increases by over 2 °C or K (200%) compared to the base case. It is noteworthy that this case also demonstrates that T_s maxima at some locations would be over 4 °C (K) higher without the cooling effect of the inflowing groundwater. Similarly, when both groundwater inflow and hyporheic exchange are neglected, simulated T_s is too high, the amplitude of diurnal temperature variations is too large, and the peak T_s occurs too early. With neither the buffering effect of hyporheic exchange nor the cooling effect of baseflow, the daily maximum T_s is more than 5 °C (K) higher than that in the base case.

These results demonstrate the importance of groundwater inflow and hyporheic exchange in creating stream reaches with thermal regimes that are capable of supporting fisheries. In fact, on the day these data were collected, the stream reach from kilometer 0.6 to 1.2 provided good habitat for rainbow trout (*Oncorhynchus mykiss*) and other cool water species because of the lower daily T_s maximum, whereas the reaches above and below are of marginal quality (*3*, *11*, *18*).

In summary, hyporheic fluxes cause a time lag and a buffering of T_s, whereas groundwater fluxes result in a depression in T_s; the differing responses of these processes reduced the problem of nonuniqueness, which facilitated manual calibration of the model and determination of these fluxes. While this manual fitting procedure is subjective, time-consuming, and requires a thorough understanding of the processes affecting T_s, it forces the analyst's intimate contact with the model, (1) helping to maintain parameter values within reasonable ranges for the stream reach, (2) allowing inclusion of "soft data" (e.g., location of hydric vegetation communities or seepage faces), that have been observed in the field, and (3) providing a clear understanding of the sensitivity of the model to its parameters.

Model-based estimating of hyporheic exchange is confounded by the fact that three separate processes can have a similar buffering effect on T_s. First, heat is carried by water flowing between the stream and the hyporheic zone. Second, heat is transferred from the flowing portion of the stream to "stagnant zones" of surface water within the stream channel. Third, heat is conducted between the stream and the subsurface sediment. In all three cases, heat is exchanged between the flowing streamwater and its surroundings (hyporheic zone, stagnant zones, and streambed conduction layer). In experiments, Gooseff et al. (*19*) observed differences in late time tailing of introduced stream tracers. They believe that these differences can be used to distinguish between the first two processes. Runkel (*20*) and others have suc-

cessfully modeled the first two of these processes by considering them together as a lumped transient storage mechanism for solutes. For heat transport in streams, the third process (streambed conduction) also influences T_s in the same manner as hyporheic and stagnant zone exchange. Because all of these processes can have nearly equivalent effects on T_s, differentiating between them using stream-temperature data alone is difficult. Thus, estimated hyporheic exchange rates may not represent hyporheic exchange alone and are likely overpredicted because they also represent heat exchange between the flowing-stream and stagnant-water zones within the channel. This is a specific example of a general concern. Error can creep into any approach that estimates flux magnitudes by simulating a response variable that is dependent on many processes; conceptual model error or uncertainty of input parameters may lead to inaccuracies of fitted parameters.

In Cottonwood Creek, groundwater inflow caused significant cooling in the restored stream reach, which was a goal of the restoration efforts. Synoptic streamflow measurements verified that groundwater inflow (baseflow) rates estimated using FLIR thermography were accurate within 10% in this application. Later in the season, streamflow decreased to zero at the upper end of the reach; however, for several weeks afterward, streamflow began between kilometers 1.0 and 1.3, which is consistent with the presence of the identified groundwater inflow zone. Furthermore, hyporheic exchange (and perhaps "stagnant zone" exchange) is shown to increase the buffering effect on T_s within the restored reach. Much of this exchange is probably a result of high conductivity riffles made of 10 cm clasts added to create pools and prevent erosion. The riffles are highly transmissive, and, at lower streamflow, all of the discharge has been observed to flow through the riffle structure, suggesting that high exchange rates are realistic. These results indicate that hydrologic function differs significantly between restored and adjacent subreaches. The increased baseflow and hyporheic exchange create a thermal regime that improves the aquatic habitat potential of the restored subreach.

Remotely sensed profiles of T_s have been combined with in situ diurnal records of T_s to gain insight into the subsurface flow system. The spatial coverage provided by the remotely sensed data enabled pinpointing abrupt changes in heat exchange and quantifying a spatially continuous baseflow contribution profile. The instream diurnal records of T_s validated the remotely sensed data and provided a continuous, temporal dataset that was used to help match the diurnal temperature cycle. Using a physically based, energy budget model, these rich data sets were used to quantify subsurface groundwater inflow and hyporheic exchanges at a restoration site where exchange rates are high relative to the streamflow. We feel the largest obstacle to scaling up this method is that the ratio of groundwater inflow and hyporheic exchange to streamflow decreases as the scale of the watershed increases. This reduces the sensitivity of the method but may be counteracted by collecting data under low-flow conditions when stream−aquifer interactions are relatively more significant. Future research should address whether this type of approach can be useful for quantifying stream−aquifer interactions at larger (watershed) scales.

Acknowledgments

This material is based upon work supported by the National Science Foundation under Grant EAR-0337393. Any opinions, findings, and conclusions or recommendations expressed in this material are ours and do not necessarily reflect the views of the NSF. A. Abeles, B. Ebel, E. Hinckley, K. Moffett, K. Rockett, and S. Violette are gratefully acknowledged for their help collecting field data. We thank Keith Loague for encouraging this project and for lending us equipment. We are grateful to FRCRM staff who familiarized us with their restoration work and provided valuable assistance. We appreciate the constructive reviews provided by the four anonymous reviewers.

Literature Cited

(1) Brunke, M.; Gonser, T. The ecological significance of exchange processes between rivers and groundwater. *Freshwater Biol.* **1997**, *37*, 1−33.

(2) Ward, J. V.; Malard, F.; Tockner, K.; Uehlinger, U. Influence of ground water on surface water conditions in a glacial flood plain of the Swiss Alps. *Hydrol. Processes.* **1999**, *13*, 277−293.

(3) Ebersole, J. L.; Liss, W. J.; Frissell, C. A.. Thermal heterogeneity, stream channel morphology, and salmonid abundance in northeastern Oregon streams. *Can. J. Fish. Aquat. Sci.* **2003**, *60*, 1266−1280.

(4) Boulton, A. J.; Findlay, S.; Marmonier, P.; Stanley, E. H.; Valett, H. M. The functional significance of the hyporheic zone in streams and rivers. *Annu. Rev. Ecol. Syst.* **1998**, *29*, 59−81.

(5) Stanford, J. A.; Ward, J. V. An ecosystem perspective of alluvial rivers: connectivity and the hyporheic corridor. *J. North Am. Benthol. Soc.* **1993**, *12*, 48−60.

(6) Rayne, S.; Henderson, G. Airborne thermal infrared remote sensing of stream and riparian temperatures in the Nicola River Watershed, British Columbia, Canada. *J. Environ. Hydrol.* **2004**, *12*, 14-1 to 14-11.

(7) Torgersen, C. E.; Price, D. M.; Li, H. W.; McIntosh, B. A. Multiscale thermal refugia and stream habitat associations of chinook salmon in northeastern Oregon. *Ecol. Appl.* **1999**, *9*, 301−319.

(8) Becker, M.; Georgian, T.; Ambrose, H.; Siniscalchi, J.; Fredrick, K. Estimating flow and flux of ground water discharge using water temperature and velocity. *J. Hydrol.* **2004**, *296*, 221−233.

(9) Mertes, L. A. Remote sensing of riverine landscapes. *Freshwater Biol.* **2002**, *47*, 799−816.

(10) Boyd, M.; Casper, B. Analytical methods for dynamic open channel heat and mass transfer. Methodology for the Heat Source model version 7.0. http://www.deq.state.or.us/wq/TMDLs/WQtools/HeatSource7.0_Methodology.pdf.

(11) Wilcox, G. Water management implications of restoring mesoscale watershed features. Presented at the International Conference on Headwater Control VI: Hydrology, Ecology and Water Resources in Headwaters, Bergen, Norway, June 20−23, 2005.

(12) Loheide, S. P.; Gorelick, S. M. A high-resolution evapotranspiration mapping algorithm (ETMA) with hydroecological applications at riparian restoration sites. *Remote Sens. Environ.* **2005**, *98*, 182−200.

(13) Rosgen, D. *Applied River Morphology*; Wildland Hydrology: Pagosa Springs, CO, 1996.

(14) Ponce, V. M.; Lindquist, D. S. Management of baseflow augmentation: a review. *Water Resour. Bull.* **1990**, *26*, 259−268.

(15) Torgersen, C. E.; Faux, R. N.; McIntosh, B. A.; Poage, N. J.; Norton D. J. Airborne thermal remote sensing for water temperature assessment in rivers and streams. *Remote Sens. Environ.* **2001**, *76* (3), 386−398.

(16) McCutcheon, S. C. *Water Quality Modeling*: *Transport and Surface Exchange in Rivers*; CRC Press: Boca Raton, FL, 1989; Vol. 1, pp 183−209.

(17) Poole, G. C.; Berman, C. An ecological perspective on in-stream temperature: natural heat dynamics and mechanisms of human-caused thermal degradation. *Environ. Manage.* **2001**, *27* (6), 787−802.

(18) Beschta, R. L.; Bilby, R. E.; Brown, G. W.; Holtby, L. B.; Hofstra, T. D. Stream temperature and aquatic habitat. In *Streamside Management*: *Forestry and Fishery Interactions*; Salo, E. O., Cundy T. W., Eds.; University of Washington: Seattle, WA, 1987; Contribution 57, pp 191−232.

(19) Gooseff, M. N.; Wondzell, S. M.; Haggerty, R.; Anderson, J. Comparing transient storage modeling and residence time distribution (RTD) analysis in geomorphically varied reaches in the Lookout Creek basin, Oregon, USA. *Adv. Water Resour.* **2003**, *26*, 925−937.

(20) Runkel, R. L. One-dimensional transport with inflow and storage (OTIS)- -A solute transport model for streams and rivers. *U. S. Geol. Surv. Water-Resour. Invest. Rep.* **1998**, *98-4018*, 73.

Received for review November 3, 2005. Revised manuscript received January 31, 2006. Accepted March 13, 2006.

ES0522074